Composites Science and Technology 167 (2018) 482–488

Contents lists available at ScienceDirect

Composites Science and Technology

journal homepage: www.elsevier.com/locate/compscitech

Effects of aspect ratio and crystal orientation of cellulose nanocrystals on properties of poly(vinyl alcohol) composite fibers

Shikha Shrestha[a], Francisco Montes[a], Gregory T. Schueneman[b], James F. Snyder[c], Jeffrey P. Youngblood[a,*]

[a] School of Materials Engineering, Purdue University, 701 West Stadium Avenue, West Lafayette, IN, 47907, United States
[b] The Forest Products Laboratory, U.S. Forest Product Service, Madison, WI, 53726, United States
[c] U.S. Army Research Laboratory, Aberdeen Proving Ground, MD, 21005, United States

ARTICLE INFO

Keywords:
Cellulose nanocrystals
Polymer-matrix reinforced composite fibers
Aspect ratios
Mechanical properties
Micromechanical modeling

ABSTRACT

This work reports a study on the effects of different types and aspect ratios of cellulose nanocrystals (CNCs) on properties of poly (vinyl alcohol) (PVA) composite fibers. CNCs were extracted from wood pulp and cotton and reinforced into PVA to produce fibers by dry-jet-wet spinning. The fibers were collected as-spun and with the first stage drawing up to draw ratio 2. The elastic modulus and tensile strength of the fibers improved with increasing CNC content (5–15 wt. %) at the expense of their strain-to-failure. It was also observed that the mechanical properties of fibers reinforced with cotton CNC were higher than the fibers with wood CNC at the same amount of CNCs due to their higher aspect ratio. The degree of orientation along the spun fiber axis was quantified by 2D X-ray diffraction. As expected, the CNC orientation correlates to the mechanical properties of the fibers. Micromechanical models were used to predict the fiber performance and compare with experimental results. Finally, surface and cross-sectional morphologies of fibers were analyzed by scanning electron microscopy and optical microscopy.

1. Introduction

In recent years, polymer nanocomposite fibers have gained popularity due to their significantly improved mechanical performances compared to neat polymer fibers [1,2]. There has been extensive research on using biodegradable or naturally derived reinforcing fillers to develop green nanocomposites in response to the high demand for alternatives to petroleum-based materials [1,3,4]. In this context, cellulose nanocrystals (CNCs) as a reinforcing agent [2,3] has a unique combination of structural properties (e.g., high stiffness and crystallinity [5,6]) and environmental-friendliness (sources include trees, bacteria, and tunicates [1,2]). CNCs are rod-like nanoparticles (length: 50–500, width: 5–20 nm) that are isolated through the controlled hydrolysis of cellulose-based materials [1,2,7]. The highly crystalline CNCs have high modulus (~110–220 GPa) and strength (~7 GPa), along with low density (~1.6 g/cm^3) [1,7]. The superior mechanical properties, biocompatibility, sustainability, and cost effectiveness of CNCs account for them having been incorporated into natural and synthetic polymer matrices, such as cellulose acetate [8], polylactic acid [9], epoxy [10], and polyvinyl alcohol [11] to obtain high-performance nanocomposites.

To take advantage of the high elastic modulus of CNC in the longitudinal axis (~110–220 GPa [1,12]), CNC reinforced composite fibers have been produced by various techniques. Clarkson et al. [9] dry spun CNC-polylactic acid fibers, reporting a two-fold increase in modulus at 5 wt.% CNC loading. Chen et al. [8] produced CNC-cellulose acetate fibers by dry spinning with an increase of 137% in tensile strength and 637% in elastic modulus. However, the experimental values are generally lower compared to those from micromechanical models in spite of the improved mechanical performance [8,13].

The previous studies showed that optimum interfacial interaction, compatibility and dispersion between CNCs and matrices strongly affected the strength of the polymer composites [4,14]. CNCs are hydrophilic [1,2,7] in nature, and hence result in reduced composite performance when combined with hydrophobic polymers due to low interfacial adhesion, poor stress transfer and severe agglomerations between the two phases [4,15,16]. Thus, water being a preferred medium for processing and dispersing CNCs in composites [17,18] makes water-soluble polyvinyl alcohol (PVA) an ideal matrix to incorporate CNCs. The hydroxyl groups in PVA form strong interfacial hydrogen bonds with CNCs and enhance their mechanical properties. PVA based fibers are commonly used in tissue scaffolding [19], drug

* Corresponding author.
E-mail address: jpyoungb@purdue.edu (J.P. Youngblood).

https://doi.org/10.1016/j.compscitech.2018.08.032
Received 2 May 2018; Received in revised form 26 July 2018; Accepted 23 August 2018
Available online 31 August 2018

delivery [20], cement composites, packaging, and others [21,22]. Incorporating CNCs into PVA fibers, which can have low strength and integrity [14,21], may facilitate improvement in mechanical properties. This approach has been taken by others. Uddin et al. [18] gel spun CNC-PVA fibers, increasing both the tensile strength (1.48GPa- l.89GPa) and elastic modulus (30GPa-56GPa). Peresin et al. [21] produced CNC-PVA fibers by electrospinning leading to more than three-fold enhancement in mechanical strength at 15% CNC loading than compared to neat PVA fibers.

There have been few studies on aspect ratio effects on cellulose-based PVA composite films [23], and to the best of our knowledge, effects of aspect ratios and types of CNCs on properties of PVA/CNC fibers (in particular) have not been experimentally studied at all. In this work, we studied the preparation and characterization of PVA-CNC fi. bers produced via dry-jet-wet spinning, which can result in more enhanced molecular alignment than conventional wet spinning [24,25] and uses less specialized equipment than gel-spinning [26]. CNCs hydrolyzed from wood and cotton were reinforced into PVA and spun into fibers. This was subsequently followed by first stage drawing up to draw ratio 2. The goal of this work is to develop industrially scalable process for composite PVA fibers with improved strength and modulus. Furthermore, experimental results for mechanical properties were compared to the predictions from micromechanical models, which accounted for CNC concentration, orientation parameter and aspectratio.

2. Materials and methods

2.1. Materials

PVA with an average molecular weight (M_w) of 89,000-98,000 and 99 + % hydrolysis was obtained from Sigma-Aldrich, St. Louis, MO. Aqueous suspensions of CNCs extracted from different sources wood pulp (2015-FPL-CNC-064; 11.8 wt. % in water) and cotton fibers (2015-FPL-CNC-081; 11.4 wt. % in water) were produced by following the same process of acid hydrolysis using sulfuric acid [27] to have a similar functionalization. To prepare different lengths from the same source requires digestion to be more aggressive and longer, which has been shown to introduce differences [1]. These CNCs with different lengths were provided by the USDA Forest Service-Forest Products Laboratory (FPL), in Madison, WI. The morphology and the average diameter of CNCs were characterized using a Philips CM-100 transmission electron microscopy (TEM) operated at 100 kV, spot size 3, 200 μm condenser aperture and 70 μm objective aperture. CNC droplets were placed on 400 mesh formvar/carbon film grid prepared with glow discharge and stained with aqueous uranyl acetate. The average dimensions of CNCs extracted from wood pulp (length: 91.7 ± 35.2 nm; diameter: 8.4 ± 7 nm) and cotton (length: 129.4 ± 34.4 nm; diameter: 9.1 ± 5.8 nm) were determined using lmageJ software. TEM images of CNCs are shown in Fig. Sl (a) and (b).

2.2. Preparation ofPVA-CNC solution

PVA solution was prepared by dissolving PVA powder in nanopure water with constant magnetic stirring at 90 °C for 3 h. As-received CNC suspensions from wood and cotton were added at O, 5, 10, 15 and 20 wt. % loadings to the solution. The mixture was transferred to a vacuum-assisted rotary evaporator, Yamato RE500, for solvent evaporation. Homogeneity of the solution was confirmed by cross-polarized optical microscopy images of spinning dopes with no discrete CNC aggregates at that length scale (Fig. S2). The solvent (water) was evaporated in the static rotary mixer (50 rpm, 80 'C and 120 psi) for 3_4h to obtain - 30 wt. % concentration of the final spinning dope.

2.3. Formation ofPVA-CNCfibers and drawing

The prepared dopes were spun using a method similar to that of Chen et al. [8] A custom-built fiber spinner based on capillary extrusion rheometer [28] with a 30° V-tapered conical shape machined to 4.38 mm was used to insert a 250 μm orifice from Bird Precision, Waltham, MA. This allows fiber processing at high shear rate of $l0^5$-10^6 $s.^{-1}$ The spinner frame was attached to an MTS Insight, a universal tensile testing machine, to control displacement rate and measure pressure. The spinning dope and the spinneret were heated at the operating temperature of 100 'C and held at the temperature for 2-4 h to degas the solution before spinning. The dope was loaded into the spinneret mounted onto the frame and the fibers were spun by pressing shaft into the reservoir. A maximum crosshead speed of 1500 mm/min was applied until the fiber started to extrude from the orifice into the ethanol bath. The air gap between the orifice and the ethanol surface was – 6 inches.

The spinning rate was controlled by the amount of force needed to maintain the fiber flow, which depends on the rheological behavior of the spinning solution. To investigate the optimal conditions for fiber formation in the spinning system, the steady state viscosity of the dopes at room temperature was measured by using a Malvern Bohlin Gemini HR Nano Rheometer with parallel plate geometry at shear rates from 1 to 100 s^{-1}. The dopes were pre-sheared for **1** min at 50 s^{-1}, and the rheology test was started after 30 s. To investigate the effects of CNC contents on the optimal conditions for fiber formation within the spinning system. At higher shear rates, the CNCs align due to their rod-like stmcture, thus, decreasing the shear viscosity of the solution. However, at higher concentrations, the suspensions change to a gel-like state (1,8]. Thus, an optimum viscosity of the spinning dope strongly depends on viscosity of polymer, concentration of CNCs, and solvents in the solution. The dopes with low viscosities formed droplets when extruded from the orifice. Hence, 100 wt.% neat CNC fibers could not be produced due to the low viscosity of 13.2 wt.% CNC solution (Fig. S3). On the contrary, high viscosity dopes produced stable fibers with a possibility of porosity defects due to the inability of voids rising to the fiber surface before solidification [8]. With the dry-jet-wet spinning configuration used in this study, the zone between dashed lines in Fig. S3 gives the approximate viscosity range at which the solution formed fibers. After fiber formation, the initial hand-drawing took place, yielding a maximum draw ratio (DR) of 2. The fibers were immersed in ethanol for 24 h followed by drying in air and in the oven at 105 'C overnight. The fibers were then stored in a desiccator before characterization.

2.4. Microscopy

Surface morphology and diameter of fibers were examined by using the images taken by a Carl Zeiss (Axio Observer Al) inverted optical microscope and measure tool in lmageJ. Fiber birefringence of CNCs was observed between crossed polarized optical filters, which is considered as a primary indicator for dispersion of CNCs. Moreover, surface and cross-sectional morphologies of fibers, before and after fracture, were determined by using a FEI XL40 scanning electron microscopy. The fiber samples were coated with gold for 30 s at 1 kV, 18 mA, using a SPI-module sputter coater.

2.5. 2D X-ray diffraction

A Bruker GADDS 2D X-ray diffractometer (2D XRD) was used to evaluate the degree of orientation of CNCs within the PVA fibers. The 2D XRD used a source of 546 nm Cua radiation at 30 mA, 20 kV for 900 s and a beam diameter of 500 μmat 6.1 cm from the detector in transmission mode. The fibers were wound, ensuring they were straight and parallel, and glued across a small plastic tab with a hole in the center. The tab with the fiber specimens was attached to a sample holder which was mounted perpendicular to the X-ray beam to allow it to pass through the fibers. The scattering patterns of fibers were recorded on a detector which was placed on the same line along with the

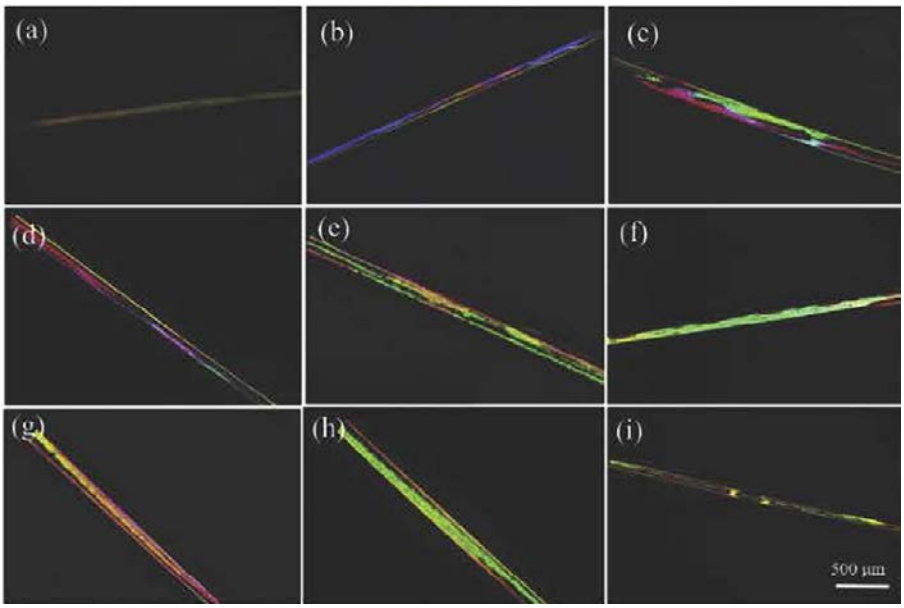

Fig. 1. Cross-polarized optical images of as-spun PVA fibers with (a) 0 wt.% CNC (b)-(e) 5, l0, 15 and 20 wt. % CNC from wood and (1)-(i) 5, 10, 15 and 20 wt.% CNC from cotton.

sample. The patterns were corrected by subtracting a backgrowid of air scattering from the raw data.

The crystal alignment of CNC was quantified by the distribution of intensity (I) with respect to azimuthal angle (¢) along the (200) crystal of the cellulose (β [29J. Hence, the integration of I versus ϕ, was obtained from 0^o to 180^o around (200) plane at $2\theta = 20\text{-}23^o$. Similarly, the crystal alignment of PVA was determined by the equatorial diffraction spots corresponding to (200) plane also at 20 = 20-23° [30,31]. Furthermore, Hermans order parameter (S) was calculated assuming axisymmetric orientation where, S = 0.0 and S = 1.0 represented no preferential orientation and a complete alignment along the axis, respectively. The equations used in these calculations are listed in the Supplementary Information (Equations (S2)-{S4)).

2. 6. *Mechanical characterization of fibers*

The mechanical properties (elastic modulus, tensile strength, and strain at failure) of a single fiber was measured using a TA Instruments Q800 Dynamic Mechanical Analysis. The fibers were attached on cardboard tabs (gauge lengths of 12-15 mm) with high strength epoxy (cured at room temperature) to avoid slippage. At least ten replicates of as-spun and drawn fibers reinforced with both types of CNCs were tested. All samples were stored in a desiccator at 23 °C and 35% RH for at least 48 h prior to testing. The mechanical properties of single fibers were tested at 0.3 N/min, applied constantly at room temperature until fracture occurred. The results *were* analyzed by using one-way analysis of variance (ANOVA) and multiple comparison Tukey tests to check for significance (at P= 0.05 level).

2. 7. *Micromechanical modeling*

Elastic modulus of PVA-CNC fibers as a function of CNC loadings was predicted by using numerous models i.e., lsost.rain, lsostress, Halpin-Tsai, and Cox-Krenchel models. Isostrain and Isostress models asswue that the reinforcing *filler* of the composites a.re continuous and perfectly aligned in one direction, and there is perfect adhesion between the filler and the polymer matrix [8]. The details are shown in the Supplementary Information (Equations (S5) and (S6)). The Halpin-Tsai model is used to determine the elastic modulus of a unidirectional short fiber composite. It is based on systems where the reinforcements are fully dispersed, aligned in the longitudinal direction and have a quantifiable aspect ratio [32,33]. This model determines the composite modulus by:

$$E_c = E_m\left(\frac{1 + \left(2^l/_D\right)\eta V_f}{1 - \eta V_f}\right) \text{where } \eta = \frac{\frac{E_f}{E_m} - 1}{\frac{E_f}{E_m} + 1} \quad (1)$$

where, E_c, E_f (143GPa) [1,8] and E_m (~4GPa, measured in this study) are tlie elastic moduli of the composite, filler (CNC) and matrix (PVA), respectively, V_f is the fiber volwue fraction determined from weight fractions and the material densities (1.26 glen? for PVA and 1.6 g/cm^3 for CNC) [1,34]. L is tlie length and D is the diameter of CNC (wood and cotton).

The modulus prediction by the Cox-Krenchel model [35,36] was developed based on a classical shear-lag model [37J. This model accowits for both aspect ratio and orientation of inclusions. The following assumptions are made in using the model for composite fibers: (i) fiber and matrix undergo elastic deformation, (ii) no axial loads on the fiber ends and (iii) fully-bonded fiber-matrix interface [35,36]. The model is governed by the equation:

$$E_c = \eta_o \eta_l V_f E_f + E_m(1 - V_f) \quad (2)$$

where, η_0 is die orientation factor, which is directly proportional to Hermans order parameter (S). η_l is the length factor and can be obtained from shear-lag model (Equation (S7)).

3. Results and discussion

3.1. *Structure and morphology of the fibers*

Fig. 1 shows polarized optical micrographs of as-spun and drawn PVA composite fibers with CNC (from wood and cotton) having concentrations of 0, 5, 10, 15 and 20 wt.%. The polarized micrographs of neat PVA fibers (Fig. 1a) show a uniform structure with little birefringence indicating low degree of orientation. CNC reinforced PVA fibers display distinct birefringence wider polarized light. It was observed that at low concentrations of 5 wt. % CNC, the fibers showed some local orientation with birefringence (Fig. 1b and f). As the CNC concentration increased, birefringence also increased showing bright colors with iridescent domains (Fig. 1c-e and g-i) associated with the

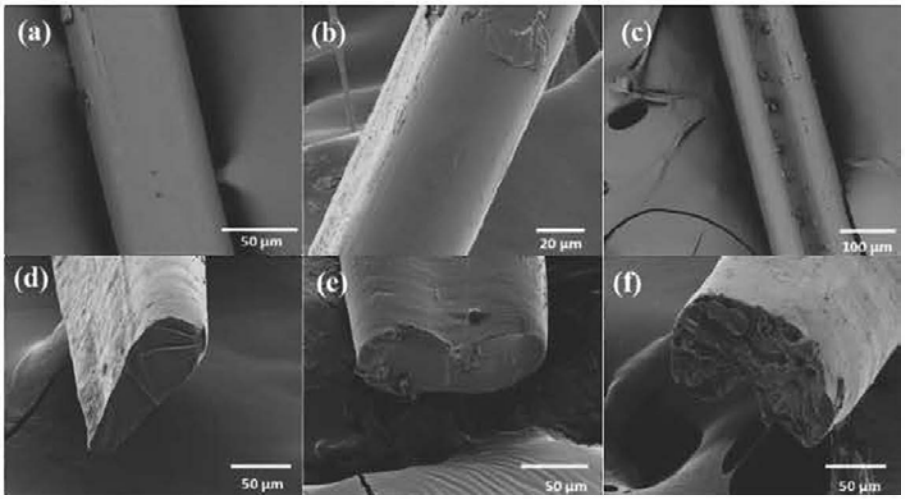

Fig. 2. SEM images of PVA-CNC fibers (a)-(c) surfaces containing CNC of 0, 15 and 20wt. %, respectively and (d)-(f) cross-sections containing CNC of 0, 10 and 20 wt. %, respectively.

anisotropy of crystalline CNC [1, 38], which indicated well-dispersed and ordered CNCs within the PVA. These images also revealed large micron scale CNC agglomerates within the PVA matrix, appearing as dark regions.

Fig. 2 shows SEM images of the surface and cross-section of the spun fibers. The average diameters of fibers with wood CNC varied between 150 and 190 μm and that with CNC cotton varied between 120 and 180 μm. The PVA fibers exhibited smooth surfaces(Fig. 2a) while PVA-CNC fibers have rough surfaces (Fig. 2b and c) as a result of CNC reinforcement. Several defects such as, porosity with higher viscosity solutions, surface irregularities, and non-cylindrical cross sections were observed. The non-uniform surfaces occur due to the faster rate of water diffusion out of the fiber than the coagulant diffusion into the fibers resulting in a skinning of more condensed material surrounding a core of less condensed giving a shell-like appearance [39]. More structural defects may be due to die non-homogenous dispersion of CNC in PVA, causing phase separation and limiting the mechanical performances at higher CNC contents. Fig. 2d shows die kidney-shaped cross-section of PVA fibers whose fractured surface was smoother than that of composite fibers. The incorporation of CNCs within die fibers introduced brittleness along with fibrils in their fractured surfaces. This fibrillation morphology was associated with the extent of orientation along the fiber axis, thus leading to higher mechanical properties. The fibrils were observed in fibers with higher CNC loadings but most prominently in the drawn fibers.

3.2. Crystal orientation of CNC within PVA-CNC fibers

The degree of CNC alignment along the fiber axis was determined by 2D XRD. Fig. 3 shows X-ray diffractograms and the integrated intensity of as-spun and drawn fibers with increasing concentration of CNC. As-spun PVA fibers exhibited anisotropic intensity around the broad Debye-Scherrer ring at (200) planes, indicating preferential alig1u11ent. Unfortwiately, die (200) peak of CNC coincides with the (200) peak of PVA preventing analysis of the individual components [13,18]. However, it can readily be seen that die anisotropy increased with increasing CNC content suggesting alig1u11ent of CNC and/or both CNC and PVA in composite fibers is induced by CNC addition. Others have shown that the elongational and shear flows induced by the conical orifice forces anisotropic particles such as CNCs to align in the direction of flow [8]. Furthermore, this alignment of CNCs can induce increased alignment of the fiber matrix polymer as well.

The degree of crystal orientation of the fibers was quantified by calculation of the Hermans order parameter (S) [40]. For PVA fibers, small S values of -0.2(as-spun) and -0.31(drawn) were observed. As CNC contents were added from 5 to 15 wt.%, the values of S increased (as spun: ~0.33 to 0.61, drawn: ~0.41 to 0.64), indicating improved alignment in the fibers, as shown in Fig. S4. However, above 15wt.% CNC, S plateaued and ultimately decreased with further addition of CNCs. This may be due to aggregates of nanocrystals at high concentrations, which hinder alignment in the flow field due to decreased effective aspect ratio as proposed for nanoparticle reinforced composites [8,16J. Furthermore, it was also observed that drawing of the fibers increased die orientation of CNCs along with the matrix PVA in the fiber axis. Since only first stage drawing of as-spun fibers was performed (up to DR = 2) in this study, the maximwu drawability of the fibers was not reached, which led to lower order parameters as compared to Peng et al. [16] and Uddin et al. [18]. Second stage post-drawing (wet or hot drawing) is highly recommended for maximum drawability of fibers in achieving higher orientation, and eventually higher order parameters.

3.3. Mechanical properties of spun fibers

The mechanical properties of the fibers with different aspect ratios of CNCs are shown in Fig. 4. It was observed that regardless of CNC types (wood or cotton), elastic modulus (E) and tensile strength (σ_{TS}) of the fibers increased along with CNC content at the expense of their strain-to-failure (ε_P). The neat as-spwi PVA fiber had an E of 3.24 GPa, σ_{TS} of 100.01 MPa and reached its ε_P at 28.31%. The E and σ_{TS} increased after adding 5-15% CNC (of both types) and reached their highest values at 15wt.% i.e., E from 3.24 to 10.76 GPa (wood) and 14.31 GPa (cotton)($P \leq 0.05$); σ_{TS} from 100.01 to 230.86 MPa (wood) and 274.38 MPa (cotton) ($P \leq 0.05$). This behavior may be due to the effective stress transfer from the PVA to CNC and formation of a continuous percolation CNC .network via hydrogen bonding [15,23J. From Fig. 4a and b, it was observed that the E and σ_{TS} of fibers with cotton CNC are higher than that of the fibers with wood CNC at the same CNC content. This is likely because the CNC with higher aspect ratio is expected to significantly improve the mechanical properties [41]. Also, as seen with die increase in crystallinity of PVA (shown by DSC data in Table S2 in Supplementary Information) by the cotton-based CNC, CNC with high aspect ratio can have strong reinforcing impact driven by crystallization of the matrix, which can also enhance the mechanical properties of the fibers [18]. However, at higher CNC content (> 15wt. %), E and σ_{TS} tend to decrease. It is probable that at higher CNC loadings, the defects such as, agglomerations, voids, and uneven cross sections increase, as shown by SEM images, leading to premature

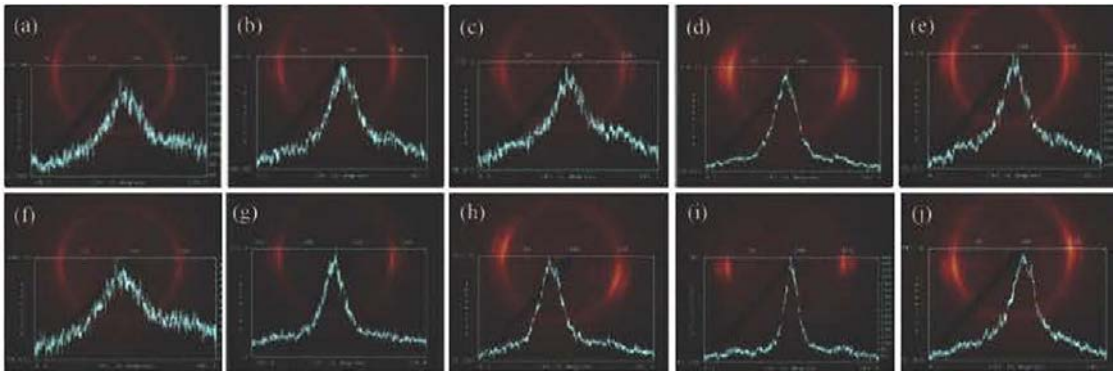

Fig. 3. 2D-XRD diffractograms of PVA-CNC (a)-(e) as-spun fibers with CNC contents of 0, 5, 10, 15 and 20wt. % and (f)-(j) drawn fibers with CNC contents of 0, 5, 10, 15 and 20 wt. %.

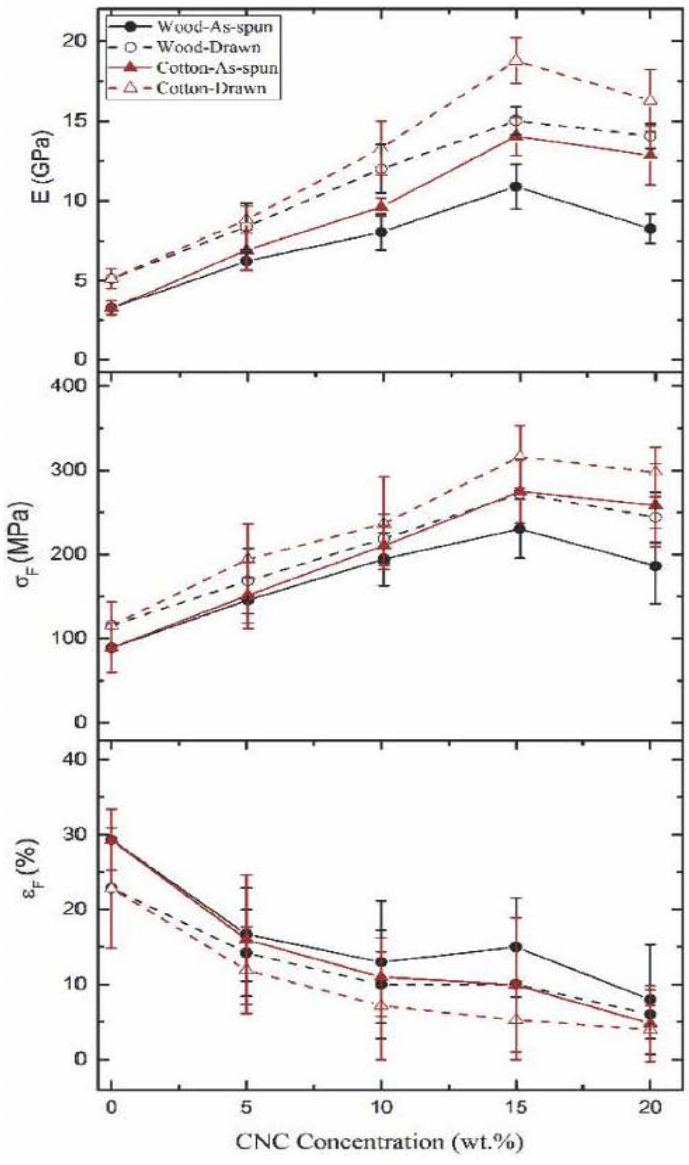

Fig. 4. Mechanical properties of as-spun and drawn PVA-CNC composite fibers: (a) elastic modulus, (b) tensile strength and (c) strain at break as a function of concentration of CNC.

failure of the fibers. There exists poor stress transfer across the interphase that resulted from CNC aggregates and voids [8,42,43J, contributing to decrease in modulus. On the other hand, it was observed that the ε_F of the fibers continuously decreased with the addition of CNCs. This is attributed to the strong interactions between CNC and PVA limiting the molecular movement of the PVA matrix [44J.

The fibers were subsequently wet-drawn (at a constant DR = 2) directly after spinning (i.e., without drying and reswelling fibers), which immensely affects the mechanical properties. As shown in Fig. 4, E and σ_{TS} for neat PVA and PVA-CNC fibers increased significantly after drawing. The maximwu E and σ_{TS} achieved (at 15 wt.% CNC content) was 15.02GPa, 272.65MPa (wood) and 18.08 GPa, 356.34 MPa (cotton), respectively ($P \leq 0.05$). Whereas, ε_P showed continuous decrease with drawing for all the fibers. The high mechanical properties of drawn fibers were induced not only by a reinforcing effect of CNCs, but also by a degree of alignment of the polymer chains along the fiber axis that originated during wet-drawing [45].

The mechanical properties of the fibers are strongly affected by the orientation of CNC. E and σ_{TS} curves are directly correlated to the order parameter curve as shown in Fig. S4. Hence, increasing CNC alignment is an important parameter to improve mechanical properties. The E of CNC in the longitudinal and transverse directions are 110-220GPa and 2-50 GPa [1,12J, respectively, which explains the increase in E with increasing order parameter. As the loading of CNC increases, the CNCs become more oriented along the fiber axis due to a strong reinforcement of CNC into PVA. However, after the maximum value of orientation is reached, the order parameter curve immediately plateaus and further addition of CNCs reduces the orientation decreasing the mechanical performances.

The improvement in mechanical properties of PVA-CNC fibers in this study is similar or higher than that reported in previous studies [18,46J. Maximum improvements in σ_{TS} of 100.03% (as-spun) and 147.5% (drawn) for wood CNC and 153.60% (as-spun) and 190.43% (drawn) for cotton CNC composite fibers were achieved. Also, maximum improvements in E of 235.38% (as-spun) and 401.94% (drawn) for wood CNC and 363.96% (as-spun) and 519.57% (drawn) for cotton CNC composite fibers were achieved. Uddin et al. [18] gel-spun PVA composite fibers up to 30 wt.% CNC, foJlowed by hot drawing. There was an increase in modulus and strength at 5 wt.% loading of CNC by 86% and 27%, respectively as compared to the neat PVA fibers [18]. Peng et al. [16J, and Liu et al. [46], showed a maximum increase of 220% and 222.9% in modulus as compared to neat PVA fibers at 5 wt.% inclusion of CNC. The results are similar to the as-spun PVA-CNC fibers at 15 wt.% CNC content in this study. The differences observed in the reinforcing effects in these fibers could be due to the differences in CNC aspect ratios or drawing. Furthermore, it was observed that the optimum concentration at which the maximum mechanical properties

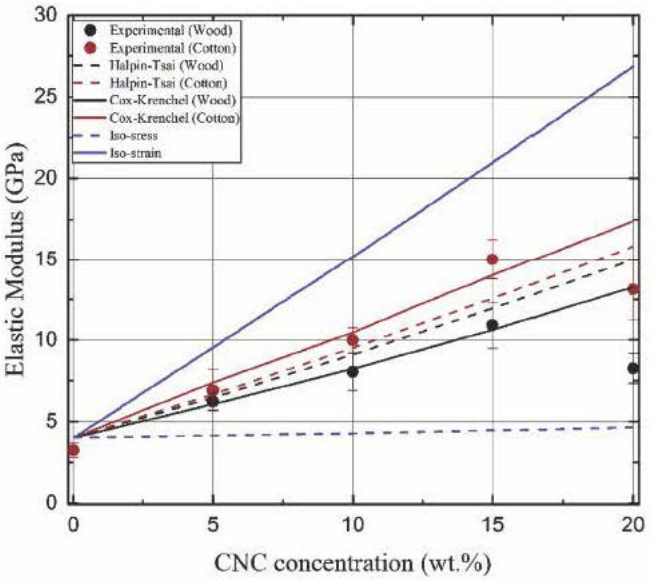

Fig. 5. Experimental and predicted values of elastic modulus for as-spun PVA-CNC fibers by Isostress, Isostrain, Halpin-Tsai and Cox-Krenchel model.

were achieved is higher in this study than the previously mentioned studies L16,18,46J. This implies that higher shear rates lead to better reinforcing potential of CNCs i.e. increase in CNC alignment along the fiber axis direction [8].

3. 4. *Micromechanical modeling of PVA-CNC fibers*

The comparison between elastic modulus from experimental data and predictions by die Isostrain, Isostress, Halpin-Tsai model and Cox-Krenchel model is shown in Fig. 5. The average aspect ratio values were determined by data collected from TEM and calculated to be 11.7 and 14.5 for CNCs extracted from wood and cotton, respectively.

Isostrain and Isostress models provide the widest upper and lower bow1ds for die PVA-CNC fiber performance, respectively. The Halpin-Tsai model showed an approximate prediction of die elastic modulus of fibers but only up to 10-12 wt.% of CNC contents. The experimental data was higher in die fibers reinforced wid1 cotton CNC d1an that predicted by the model at 15 wt.% CNC. The increase in modulus may be due to increased crystallinity of PVA induced by die CNCs. On contrary, the model over-predicted die performai1ce of die fibers above 15 wt.%. The divergence at higher CNC content was possibly due to die agglomerations between CNCs resulting in a larger sized reinforcement, which cannot be predicted by any model. This significantly lowers the filler-matrix surface area leading to decrease in mechanical properties [47J.

The Cox-Krenchel model is based on the aligned reinforcing phase along die fiber axis and its aspect ratio [8,35,36]. The prediction by this model showed the best agreement with die experimental modulus than a11y od1er models used in d1is study. Moreover, the model assumed perfect elastic adhesion between the filler a11d matrix. Thus, die good fit is indicative of a high degree of interaction between CNC and PVA. Hence, die PVA composite fibers showed a11 improved dispersion along wid1 higher elastic modulus [48J. However, die deviation at die higher CNC content is related with die defects, such as CNC agglomerates as discussed above.

The general fitting of the models demonstrated the importance of good dispersion of CNCs, alignment of reinforcement and matrix (CNC/PVA) and crystallinity of the matrix (which is affected by the CNC content) to improve the mechanical properties of the fibers [8,13J. Further increment of CNC above its optimum concentration decreases CNC dispersion, which limits improvement of modulus. Importa11tly, the models indicate that shear-lag behavior is dominant.

4. Conclusions

CNCs derived from wood pulp and cotton were reinforced into PVA to produce continuous fibers by dry-jet-wet spinning, followed by wet-drawing. Tensile strength and elastic modulus of the fibers were greatly improved by adding both types CNC up to 15 wt.%, after which the properties plateaued or decreased, possibly due to defect formation from a loss in CNC dispersion. The drawn fibers also exhibited highly oriented CNC and excellent mechanical properties. It was observed that the lengths of CNCs have significant beneficial effect on the mechanical strength of die matrix. Micromechanical models suggest that the increase in elastic modulus of PVA-CNC fiber resulted from high interfacial interaction between CNC and PVA, increased orientation parameter, greater aspect ratios and that the CNCs observed shear-lag behavior. Overall, this study suggested that cotton CNC exhibited better intrinsic properties than wood CNC, in terms of reinforcing PVA, due to their modest increase in aspect ratios that have outsized effect owing to die structural arrangement of the CNC in the polymer (i.e. shear-lag rather than percolation).

Acknowledgements

The authors would like to acknowledge financial support from the Private-Public Partnership for Nanotechnology in the Forestry Sector (P3Nano) under grant number 107563 a11d 107528.

Appendix A. Supplementary data

Supplementary data related to this article ca11 be fow1d at https://doi.org/10.1016/j.compscitech.2018.08.032.

Reference

[1] R.J. Moon, A. Martini, J. Nairn, J. Simonsen, J. Youngblood, Cellulose nanomaterials review: structure, properties and nanocomposites, Chem. Soc. Rev. 40 (2011) 3941.
[2] M.A.S. Azizi Samir, F. Alloin, A. Dufresne, Review of recent research into cellulosic whiskers, their properties and their application in nanocomposite field, Biomacromolecules 6 (2005) 612–626.
[3] G. Siqueira, J. Bras, A. Dufresne, Cellulose whiskers versus microfibrils: influence of the nature of the nanoparticle and its surface functionalization on the thermal and mechanical properties of nanocomposites, Biomacromolecules 10 (2009) 425–432.
[4] A. Bledzki, Composites reinforced with cellulose based fibres, Prog. Polym. Sci. 24 (1999) 221–274.
[5] J.A. Diaz, X. Wu, A. Martini, J.P. Youngblood, R.J. Moon, Thermal expansion of self-organized and shear-oriented cellulose nanocrystal films, Biomacromolecules 14 (2013) 2900–2908.
[6] S. Shrestha, J.A. Diaz, S. Ghanbari, J.P. Youngblood, Hygroscopic swelling determination of cellulose nanocrystal (CNC) films by polarized light microscopy digital image correlation, Biomacromolecules 18 (2017) 1482–1490.
[7] Y. Habibi, L.A. Lucia, O.J. Rojas, Cellulose nanocrystals: chemistry, self-assembly, and applications, Chem. Rev. 110 (2010) 3479–3500.
[8] S. Chen, G. Schueneman, R.B. Pipes, J. Youngblood, R.J. Moon, Effects of crystal orientation on cellulose nanocrystals–cellulose acetate nanocomposite fibers prepared by dry spinning, Biomacromolecules 15 (2014) 3827–3835.
[9] C.M. Clarkson, J.P. Youngblood, Dry-spinning of cellulose nanocrystal/polylactic acid composite fibers, Green Mater. (2018) 1–33.
[10] S.X. Peng, S. Shrestha, Y. Yoo, J.P. Youngblood, Enhanced dispersion and properties of a two-component epoxy nanocomposite using surface modified cellulose nanocrystals, Polymer (Guildf) 112 (2017) 359–368.
[11] M.S. Peresin, Y. Habibi, J.O. Zoppe, J.J. Pawlak, O.J. Rojas, Nanofiber composites of polyvinyl alcohol and cellulose nanocrystals: manufacture and characterization, Biomacromolecules 11 (2010) 674–681.
[12] F.L. Dri, L.G. Hector, R.J. Moon, P.D. Zavattieri, Anisotropy of the elastic properties of crystalline cellulose Iβ from first principles density functional theory with Van der Waals interactions, Cellulose 20 (2013) 2703–2718.
[13] W.J. Lee, A.J. Clancy, E. Kontturi, A. Bismarck, M.S.P. Shaffer, Strong and stiff: high-performance cellulose nanocrystal/poly(vinyl alcohol) composite fibers, ACS Appl. Mater. Interfaces 8 (2016) 31500–31504.
[14] B. Tan, Y. Ching, S. Poh, L. Abdullah, S. Gan, A review of natural fiber reinforced poly(vinyl alcohol) based composites: application and opportunity, Polymers (Basel) 7 (2015) 2205–2222.
[15] A. Ramezani Kakroodi, S. Cheng, M. Sain, A. Asiri, Mechanical, thermal, and

morphological properties of nanocomposites based on polyvinyl alcohol and cellulose nanofiber from aloe vera rind, J. Nanomater. (2014) 1–7.
[16] J. Peng, T. Ellingham, R. Sabo, L.-S. Turng, C.M. Clemons, Short cellulose nanofibrils as reinforcement in polyvinyl alcohol fiber, Cellulose 21 (2014) 4287–4298.
[17] V. Favier, H. Chanzy, J.Y. Cavaillé, Polymer nanocomposites reinforced by cellulose whiskers, Macromolecules 28 (1995) 6365–6367.
[18] A. Jalal Uddin, J. Araki, Y. Gotoh, Toward "strong" green nanocomposites: polyvinyl alcohol reinforced with extremely oriented cellulose whiskers, Biomacromolecules 12 (2011) 617–624.
[19] L. Yao, T.W. Haas, A. Guiseppi-Elie, G.L. Bowlin, D.G. Simpson, G.E. Wnek, Electrospinning and stabilization of fully hydrolyzed poly(vinyl alcohol) fibers, Chem. Mater. 15 (2003) 1860–1864.
[20] E.-R. Kenawy, G.L. Bowlin, K. Mansfield, J. Layman, D.G. Simpson, E.H. Sanders, G.E. Wnek, Release of tetracycline hydrochloride from electrospun poly(ethylene-co-vinylacetate), poly(lactic acid), and a blend, J. Contr. Release 81 (2002) 57–64.
[21] M. Peresin, Y. Habibi, J. Zoppe, J. Pawlak, O. Rojas, Nanofiber composites of polyvinyl alcohol and cellulose nanocrystals: manufacture and characterisation, Biomacromolecules 11 (2010) 674–681.
[22] A. Koski, K. Yim, S. Shivkumar, Effect of molecular weight on fibrous PVA produced by electrospinning, Mater. Lett. 58 (2004) 493–497.
[23] K. Yuwawech, J. Wootthikanokkhan, S. Tanpichai, Effects of two different cellulose nanofiber types on properties of poly(vinyl alcohol) composite films, J. Nanomater. 2015 (2015) 1–10.
[24] C. Clemons, Nanocellulose in spun continuous fibers: a review and future outlook, J. Renew. Mater. 4 (2016) 327–339.
[25] V. Gabara, J.D. Hartzler, K.S. Lee, Aramid fibers, in: M. Lewin (Ed.), Handb. Fiber Chem. third ed., Taylor & Francis, New York, 2007, pp. 1006–1007 Boca Raton, FL.
[26] H. Yasuda, K. Ban, Y. Ohta, Gel Spinning Processes, Woodhead Publishing Limited, 1994.
[27] M.S. Reid, M. Villalobos, E.D. Cranston, Benchmarking cellulose nanocrystals: from the laboratory to industrial production, Langmuir (2017) 1583–1598.
[28] I.O. Salyer, J.W. Heyd, R.M. Brodbeck, L.W. Hartzel, L.E. Brown, Use of a capillary extrusion rheometer to measure curing of thermosetting plastics and rubbers, J. Polym. Sci. - Part A Gen. Pap. 3 (1965) 1911–1939.
[29] Y. Nishiyama, P. Langan, H. Chanzy, Crystal structure and hydrogen-bonding system in cellulose Iβ from synchrotron X-ray and neutron fiber diffraction, J. Am. Chem. Soc. 124 (2002) 9074–9082.
[30] A.J. Uddin, M. Fujie, S. Sembo, Y. Gotoh, Outstanding reinforcing effect of highly oriented chitin whiskers in PVA nanocomposites, Carbohydr. Polym. 87 (2012) 799–805.
[31] J.D. Cho, W.S. Lyoo, S.N. Chvalun, J. Blackwell, X-ray analysis and molecular modeling of poly(vinyl alcohol)s with different stereoregularities, Macromolecules 32 (1999) 6236–6241.
[32] J.C. Halpin, S.W. Tsai, Effects of Environmental Factors on Composite Materials, (1969).
[33] W. Helbert, J.Y. Cavaille, A. Dufresne, U.J. Fourier, Thermoplastic nanocomposites filled with straw cellulose whiskers . Part I : processing and mechanical behavior, Polym. Compos. 17 (1996) 604–611.
[34] N.A. Peppas, E.W. Merrill, Poly(vinyl alcohol) hydrogels: reinforcement of radiation-crosslinked networks by crystallization, J. Polym. Sci. Polym. Chem. Ed. 14 (1976) 441–457.
[35] H.L. Cox, The elasticity and strength of paper and other fibrous materials, Br. J. Appl. Phys. 3 (1952) 72–79.
[36] H. Krenchel, Fibre Reinforcement, Akademisk Forlag, Copenhagen, Denmark, 1964.
[37] J.N. Coleman, M. Cadek, R. Blake, V. Nicolosi, K.P. Ryan, C. Belton, A. Fonseca, J.B. Nagy, Y.K. Gun'ko, W.J. Blau, High performance nanotube-reinforced plastics: understanding the mechanism of strength increase, Adv. Funct. Mater. 14 (2004) 791–798.
[38] J.-F. Revol, L. Godbout, X.-M. Dong, D.G. Gray, H. Chanzy, G. Maret, Chiral nematic suspensions of cellulose crystallites; phase separation and magnetic field orientation, Liq. Cryst. 16 (1994) 127–134.
[39] M. Elices, J. Llorca, Fiber Fracture, Elsevier Science Ltd, Kidlington, 2002.
[40] S. Park, J.O. Baker, M.E. Himmel, P.A. Parilla, D.K. Johnson, Cellulose crystallinity index: measurement techniques and their impact on interpreting cellulase performance, Biotechnol. Biofuels 3 (2010) 10.
[41] M. Mariano, C. Chirat, N. El Kissi, A. Dufresne, Impact of cellulose nanocrystal aspect ratio on crystallization and reinforcement of poly(butylene adipate-co-terephthalate), J. Polym. Sci., Part B: Polym. Phys. 54 (2016) 2284–2297.
[42] J. Lu, T. Wang, L.T. Drzal, Preparation and properties of microfibrillated cellulose polyvinyl alcohol composite materials, Composer Part A Appl. Sci. Manuf. 39 (2008) 738–746.
[43] W. Zhang, X. He, C. Li, X. Zhang, C. Lu, X. Zhang, Y. Deng, High performance poly (vinyl alcohol)/cellulose nanocrystals nanocomposites manufactured by injection molding, Cellulose 21 (2014) 485–494.
[44] D. Cheng, Y. Wen, X. An, X. Zhu, Y. Ni, TEMPO-oxidized cellulose nanofibers (TOCNs) as a green reinforcement for waterborne polyurethane coating (WPU) on wood, Carbohydr. Polym. 151 (2016) 326–334.
[45] R. Endo, T. Saito, A. Isogai, TEMPO-oxidized cellulose nanofibril/poly(vinyl alcohol) composite drawn fibers, Polymer (Guildf). 54 (2013) 935–941.
[46] D. Liu, J. Li, F. Sun, R. Xiao, Y. Guo, J. Song, Liquid crystal microphase separation of cellulose nanocrystals in wet-spun PVA composite fibers, RSC Adv. 4 (2014) 30784.
[47] X. Miao, F. Tian, J. Lin, H. Li, X. Li, F. Bian, X. Zhang, Tuning the mechanical properties of cellulose nanofibrils reinforced polyvinyl alcohol composites via altering the cellulose polymorphs, RSC Adv. 6 (2016) 83356–83365.
[48] P. Dhar, D. Tarafder, A. Kumar, V. Katiyar, Effect of cellulose nanocrystal polymorphs on mechanical, barrier and thermal properties of poly(lactic acid) based bionanocomposites, RSC Adv. 5 (2015) 60426–60440.